Supporting Information

Schulz et al. 10.1073/pnas.1620636114

DXM Concentration Profiles from X-Ray Microscopy

The DXM concentration profiles are generated by soft X-ray absorption spectromicroscopy, which is a label-free technique that yields 2D absolute concentration profiles in thin skin slabs with a lateral resolution below 100 nm (15).

In the sample after 1,000-min penetration time the SC is not aligned perpendicularly with respect to the z axis, as seen in Fig. S1*A*. Therefore, we first apply an affine transformation and shear the 2D profile until the SC is perpendicular to the z axis; the resulting aligned 2D transmission intensity profile is shown in Fig. S1*B*.

Absolute DXM concentration profiles are derived from the transmission intensity profiles at two different photon energies as described before (15). The resulting 2D DXM concentration profiles at three different penetration times are shown in Fig. S2. For the theoretical analysis we average the 2D concentration profiles along the lateral position x. The resulting 1D concentration profiles are shown in the main text.

To import the experimental data into the inverse diffusion-equation modeling, we apply cubic smoothing splines. This is accomplished by minimizing the sum

$$\sum_{i=1}^{N_k^{\text{data}}} \lambda(c(z_i)-c_s(z_i))^2+(1-\lambda)(c_s(z_{i-1})-2c_s(z_i)+c_s(z_{i+1}))^2 \quad \textbf{[S1]}$$

for the 10-min, 100-min, and 1,000-min profiles, where N_k^{data} is the number of data points in the kth dataset, $c(z)$ is the experimental 1D-concentration profile, and $c_s(z)$ is a cubic spline function that serves as an estimator for $c(z)$. The smoothing parameter λ is set to $\lambda=0.02$, which leads to a sufficient smoothing of the cubic splines, as seen in the main text. We used the cubic smoothing spline function implemented in Matlab.

Variable Discretization of the 1D Diffusion Equation

For modeling of the diffusion, we separate the total system into three layers, the HEC gel, the epidermis, and the layer underneath that includes the dermis and parts of the subcutaneous fat layer. Experimental measurements are available within the epidermis only over a thickness of ≈80 μm. The HEC gel layer and the subepidermal layer (which is called dermis in the remainder of this article for brevity) have thicknesses of 0.4 mm and 2 cm, respectively. We use a constant discretization width of 1 μm for the epidermis and variable discretization width in the HEC gel and the dermis. Note that the free energy and the diffusivity are assumed to be constant in the HEC gel and in the dermis. For constant free energy and diffusivity the diffusion equation reduces to

$$\frac{\partial c(t,z)}{\partial t}=D\frac{\partial^2 c(t,z)}{\partial z^2}. \quad \textbf{[S2]}$$

We derive a discretized version of Eq. **S2** for a nonuniform discretization of the spatial coordinate z. Let $\Delta_i=z_i-z_{i-1}$ be the distance between two discretization points. Performing a Taylor expansion up to second order yields

$$c(z_{i+1})=c(z_i)+\Delta_{i+1}\frac{\partial c(z_i)}{\partial z}+\frac{1}{2}\Delta_{i+1}^2\frac{\partial^2 c(z_i)}{\partial z^2}+O(\Delta_{i+1}^3) \quad \textbf{[S3]}$$

$$c(z_{i-1})=c(z_i)-\Delta_i\frac{\partial c(z_i)}{\partial z}+\frac{1}{2}\Delta_i^2\frac{\partial^2 c(z_i)}{\partial z^2}+O(\Delta_i^3). \quad \textbf{[S4]}$$

Multiplying the first equation with Δ_i and the second equation with Δ_{i+1} and adding both equations gives for the second derivative

$$D\frac{\partial^2 c(z_i)}{\partial z^2}=2D\Big(\frac{1}{\Delta_{i+1}(\Delta_{i+1}+\Delta_i)}c_{i+1}-\frac{1}{\Delta_{i+1}\cdot\Delta_i}c_i+\frac{1}{\Delta_i(\Delta_{i+1}+\Delta_i)}c_{i-1}\Big) \quad \textbf{[S5]}$$

$$=W_{i,i+1}c_{i+1}+W_{i,i}c_i+W_{i,i-1}c_{i-1}, \quad \textbf{[S6]}$$

from which we can read off the rates

$$W_{i,i+1}=2D\frac{1}{\Delta_{i+1}(\Delta_{i+1}+\Delta_i)} \quad \textbf{[S7]}$$

$$W_{i,i}=-2D\frac{1}{\Delta_{i+1}\cdot\Delta_i} \quad \textbf{[S8]}$$

$$W_{i,i-1}=2D\frac{1}{\Delta_i(\Delta_{i+1}+\Delta_i)}. \quad \textbf{[S9]}$$

Using Eq. **S6** we numerically solve the diffusion equation for variable discretization widths in areas of constant free energy and diffusivity. In areas of nonconstant free energy and diffusivity but equidistant discretization width, we use the discretization given in the main text.

Trust-Region Optimization for Constrained Nonlinear Problems

To obtain the profiles for the free energy $F(z)$ and diffusivity $D(z)$ from the given experimental concentration profiles, we introduce the sum of the squared residuals

$$\sigma^2=\frac{1}{N_p}\sum_{k=1}^{N_p}\frac{1}{N_k^{\text{data}}}\sum_{i=1}^{N_k^{\text{data}}}\left(c_i^{\text{exp}}(t_k)-\sum_{j=1}^{N}\mathrm{e}_{i,j}^{t_k\mathbb{W}}c_j(0)\right)^2 \quad \textbf{[S10]}$$

$$=\mathbf{R}^T\mathbf{R}=r_1^2+r_2^2+\ldots+r_{N_{\text{data}}}^2, \quad \textbf{[S11]}$$

where $\mathbf{R}(\mathbf{x})$ is the residual vector containing the errors of the predicted and observed concentrations as a function of $\mathbf{x}=\mathbf{x}(F_1,\ldots,F_{N_{\text{param}}},D_1,\ldots,D_{N_{\text{param}}})$. The vector $\mathbf{x}$ has $2N_{\text{param}}$ and the residual vector has $N_{\text{data}}=\sum_{k=1}^{N_p}N_k^{\text{data}}$ components.

To minimize Eq. **S11** we approximate σ^2 by a first-order Taylor expansion

$$\sigma^2(\mathbf{x}+\mathbf{d})=Q(\mathbf{d})\approx\mathbf{R}^T(\mathbf{x}+\mathbf{d})\mathbf{R}(\mathbf{x}+\mathbf{d}) \quad \textbf{[S12]}$$

with $\mathbf{R}(\mathbf{x}+\mathbf{d})\approx\mathbf{R}(\mathbf{x})+\mathbb{J}_R(\mathbf{x})\mathbf{d}$, where $\mathbb{J}$ describes the Jacobian of $\mathbf{R}$ at $\mathbf{x}$ and gives for Q

$$Q(\mathbf{d})=\sigma^2(\mathbf{x})+\left(\mathbb{J}^T\mathbf{R}(\mathbf{x})\right)^T\mathbf{d}+\frac{1}{2}\mathbf{d}^T\mathbb{J}^T\mathbb{J}\mathbf{d}, \quad \textbf{[S13]}$$

with $\mathbb{J}^T\mathbf{R}(\mathbf{x})$ denoting the gradient of $\sigma^2(\mathbf{x})$ and $\mathbb{J}^T\mathbb{J}$ approximating the Hessian of $\sigma^2(\mathbf{x})$. To obtain a new approximation in the next iteration step $\mathbf{x}^{m+1}=\mathbf{x}^m+\mathbf{d}$, we trust the approximation $Q(\mathbf{d})$ only within a trust-region radius Δ^m depending on the current iteration step m. We state the following trust-region problem,

$$\text{Find}\quad\min\quad Q(\mathbf{d})\quad\text{under the constraint}\quad||\mathbb{D}^{-1}\mathbf{d}||<\Delta^m, \quad \textbf{[S14]}$$

where $\mathbb{D}$ is a scaling matrix that transforms constraints we assume on the solution space of $\mathbf{x}$ or $\mathbf{d}$ into an unconstrained problem $\mathbf{d}_{unc.}=\mathbb{D}^{-1}\mathbf{d}$. Note that two kinds of constraints are introduced:

(*i*) One comes from restricting the parameter space $\mathbf{x}$ to a subspace of $\mathbf{x}$ and (*ii*) the other constraint comes from minimizing the function $Q(\mathbf{d})$ only within a trust-region Δ. How accurately $\sigma^2(\mathbf{x})$ is approximated by $Q(\mathbf{d})$ can be estimated by the reduction value

$$r^m = \frac{\sigma^2(\mathbf{x}) - \sigma^2(\mathbf{x}+\mathbf{d})}{\sigma^2(\mathbf{x}) - Q(\mathbf{d})}, \qquad \text{[S15]}$$

where the numerator describes the actual reduction and the denominator the predicted reduction. If r is close to 1, the approximation is good and the step $\mathbf{x}^m + \mathbf{d}$ is accepted with an increase of the trust-region Δ^m. If the approximation is bad, then $\mathbf{x}^{m+1} = \mathbf{x}^m$ and the trust region will be decreased.

Finding the minimum of $Q(\mathbf{d})$ within the trust-region radius Δ could be done by applying the Gauss–Newton or steepest-descent algorithm to Q, which would involve solving a linear system. We use a so-called dogleg strategy for trust-region problems that is a hybrid of Gauss–Newton and steepest descent. First, we calculate the steepest-descent direction and find the steepest point—the Cauchy point—along that direction within the trust-region radius. From the Cauchy point we calculate the vector pointing to the Gauss–Newton point. The intersection between that vector and the trust-region boundary is the new point $\mathbf{x}^{m+1}$. We assume no constraints for F but constrain D to $D \in (0, 10^4]$ $\mu m^2/s$, where the upper bound is four times larger than the diffusion constant of DXM in water. A total of 1,000 runs with 250 iterations per run are performed where only the best 1% of solutions are kept for further analysis. We use the trust-region reflective routine implemented in Matlab.

Calculating the DXM Penetration Amount from Estimated *F(z)* and *D(z)* Profiles

The penetrated amount in the epidermis at time t is calculated by

$$C_{\text{epi}}(t) = \int_{0\ \mu m}^{80\ \mu m} c(z,t)\,dz, \qquad \text{[S16]}$$

where $c(z,t)$ is approximated by $e_{i,j}^{t\mathbb{W}} c_j(0)$. This yields at time $t = 1{,}000$ min an epidermal DXM amount of ≈ 471.9 $\mu g/cm^2$. The amount in the dermis at the same time follows as

$$C_{\text{derm}}(t = 1{,}000\text{ min}) = \int_{80\ \mu m}^{2\ cm} c(z)\,dz \approx 1.2\ \mu g/cm^2. \qquad \text{[S17]}$$

In the stationary long-time limit the distribution of DXM can be calculated from the free energy alone. The integrated amount of DXM in the dermis in the long-time limit is determined by

$$C_{\text{derm}}^{\text{eq}} = 600\ \mu g/cm^2 \cdot \frac{1}{Z} \cdot \int_{80\ \mu m}^{2\ cm} e^{-\beta F(z)}\,dz \approx 10.0\ \mu g/cm^2, \qquad \text{[S18]}$$

where the normalization factor is given by

$$Z = \int_{-400\ \mu m}^{2\ cm} e^{-\beta F(z)}\,dz. \qquad \text{[S19]}$$

Analogously, the stationary amount in the epidermis follows as $C_{\text{epi}}^{\text{eq}} \approx 465.0$ $\mu g/cm^2$ and in the gel as $C_{\text{gel}}^{\text{eq}} \approx 125.0$ $\mu g/cm^2$.

Estimate of Free-Energy Barrier Height Between Epidermis and Dermis

In Fig. S3*A* the error σ of the residual is plotted as a function of the free-energy barrier height $\Delta F_{\text{VE/derm}}$ between viable epidermis and dermis. The error decreases with increasing barrier height and reaches a minimum value of $\sigma \approx 0.57 \mu g/(cm^2 \cdot \mu m)$, indicated by a horizontal dashed line, for a barrier height of $\Delta F_{\text{VE/derm}} = 20.5$ kJ/mol. For larger barrier height the error stays roughly constant, and we conclude that the value $\Delta F_{\text{VE/derm}} = 20.5$ kJ/mol constitutes a lower bound for the free-energy barrier between the viable epidermis and the dermis.

The influence of varying values of $\Delta F_{\text{VE/derm}}$ on the DXM concentration profile in the epidermis for 1,000-min penetration time is shown in Fig. S3*B*. For small values of $\Delta F_{\text{VE/derm}}$ the predicted concentration profile is much lower than the experimental profile, which is shown by a dotted line. Only the profiles for $\Delta F_{\text{VE/derm}} = 15$ kJ/mol (green line) and $\Delta F_{\text{VE/derm}} = 20.5$ kJ/mol (red line) get close to the experimental profile.

The same conclusion can be drawn from the integrated DXM amount in the epidermis, which is shown in Fig. S3*C*. For low free-energy barrier $\Delta F_{\text{VE/derm}}$ the integrated DXM amount is much lower than the experimental one because DXM easily penetrates into the dermis. This can in particular be seen for $\Delta F_{\text{VE/derm}} = 0, 5, 10$ kJ/mol, for which most of the DXM will have penetrated into the dermis and below. We conclude that a sufficient barrier height is crucial to hinder DXM penetration into the dermis.

Bootstrapping Analysis

In the following we do not use the full experimental dataset to derive the underlying free-energy and diffusivity profiles. Instead, we reduce the input dataset for one penetration time. As described in the main text, there are 164 free-energy and diffusivity parameters we need to estimate. The total number of experimental concentration input data points is $73 + 80 + 80 = 233$. For a least-squares algorithm it is important that the number of input data points is equal to or larger than the number of unknown parameters; otherwise the matrix $\mathbb{J}^T\mathbb{J}$ is not invertible and the Gauss–Newton step cannot be performed. If we omit the entire 10-min profile, which consists of 73 data points, we would end up with 160 input data points and thus an underdetermined system. The same holds true for omitting the 100-min and 1,000-min samples. Therefore, we do not omit an entire profile, but rather omit every data point of that profile except the data in the SC, which contributes with 12 data points.

The minimization protocol is the same as used in the main text: 1,000 runs with 250 iterations, a constant free-energy landscape, and arbitrarily chosen diffusivity values D in the interval $[10^{-1}, \ldots, 10^3]$ $\mu m^2/s$ are used as an initial guess. Only the best 1% of solutions with the smallest error σ are considered. In Fig. S4 the estimated free-energy and diffusivity profiles and the predicted concentration profiles are shown. When reducing the 10-min input dataset, we still get accurate results for the concentration profile in the SC, but a higher concentration in the viable epidermis is predicted at 10-min penetration time. For 100-min and 1,000-min penetration times the prediction is very accurate compared with the experimental data. The error is calculated to be $\sigma = 0.7$ $\mu g/(cm^2 \cdot \mu m)$ and thus is only slightly higher than for the case with complete input data, leading to an error of $\sigma = 0.6 \mu g/(cm^2 \cdot \mu m)$.

When reducing the 100-min input dataset, there is good agreement for the profiles at 10-min and 1,000-min penetration times, but the 100-min profile understandably shows larger deviations. The error is $\sigma = 0.7$ $\mu g/(cm^2 \cdot \mu m)$.

When reducing the 1,000-min input dataset in the minimization procedure, the agreement for the 10-min profile and the 100-min profile is good with an error of $\sigma = 0.7$ $\mu g/(cm^2 \cdot \mu m)$, but as one would expect, the deviations at a penetration time of 1,000 min are larger.

The free energy profiles for all three reduced-input datasets are quite similar to each other.

All diffusivity profiles for the reduced 10-min, 100-min, and 1,000-min input data sets show very similar profiles, especially in the SC region. Only the profile for the reduced 10-min dataset shows deviations in the SG, where the diffusivity is predicted to be of the same magnitude as in the VE, which explains why more substance has penetrated through the SC into the VE. We conclude that even with reduced-input data, the estimated free-energy and diffusivity profiles reproduce the experimental concentration profiles at different times in a satisfactory manner.

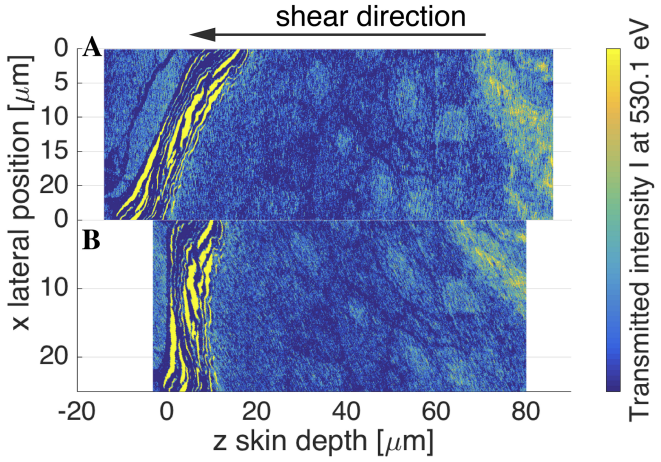

Fig. S1. (*A*) Two-dimensional transmission intensity profile at photon energy $E = 530.1$ eV after 1,000-min penetration time taken directly from X-ray microscopy. The SC is not aligned perpendicularly to the *z* axis. (*B*) Aligned 2D intensity profile after shearing along the *z* axis.

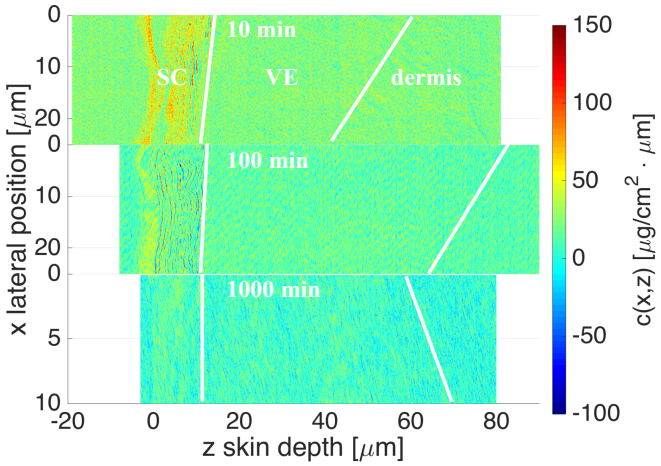

Fig. S2. Experimental 2D concentration profiles obtained after 10-min, 100-min, and 1,000-min penetration times. The 1,000-min profile has been sheared to achieve perpendicular orientation of the SC with respect to the *z* axis. In the 10-min and 100-min profiles the inhomogeneous distribution of DXM within the SC is well observed.

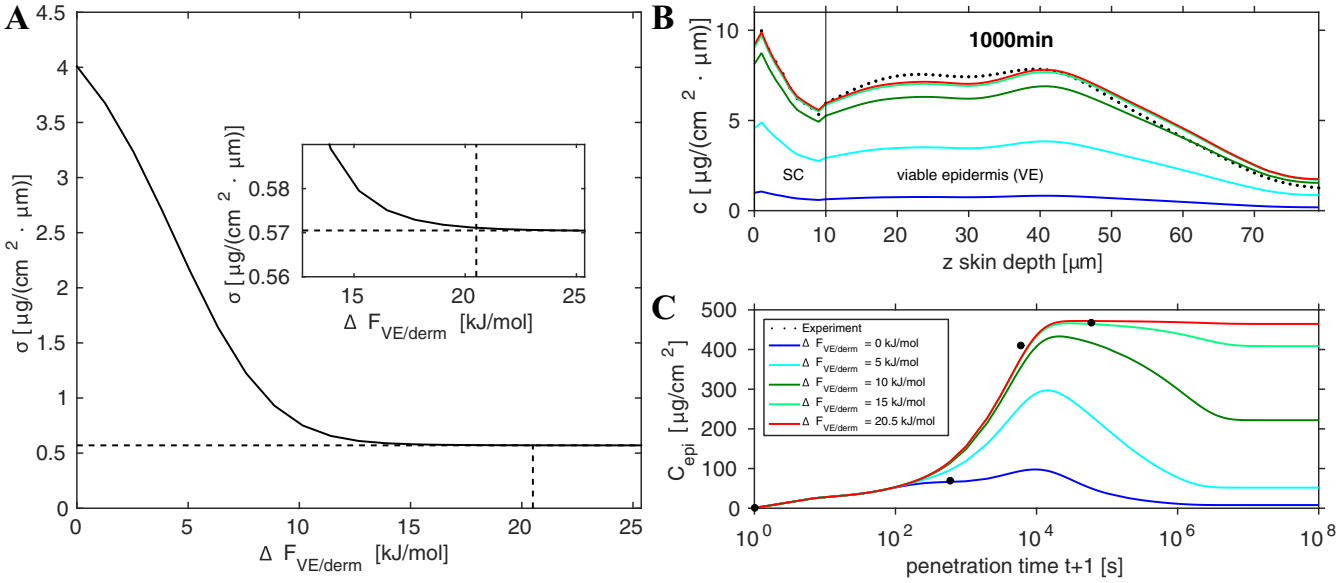

Fig. S3. Effect of varying free-energy barrier height $\Delta F_{VE/derm}$ between VE and dermis. (*A*) Residual error σ as a function of $\Delta F_{VE/derm}$. The minimal error $\sigma = 0.571$ µg/(cm^2 µm) is indicated by a dashed horizontal line, which is reached for a free-energy barrier of $\Delta F_{VE/derm} = 20.5$ kJ/mol, which is indicated by a vertical dashed line. (*B*) The 1,000-min concentration profiles calculated for different barrier heights $\Delta F_{VE/derm}$. (*C*) Integrated amount of DXM in epidermis for different barrier heights $\Delta F_{VE/derm}$.

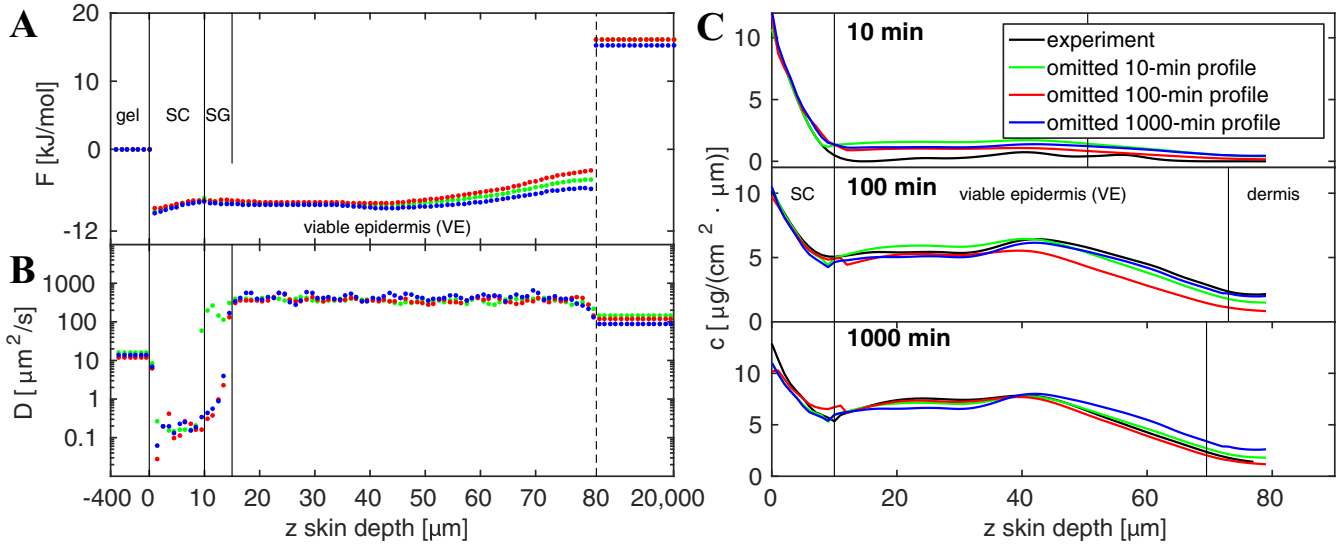

Fig. S4. Bootstrapping. Reducing the input datasets at 10-min, 100-min, or 1,000-min penetration time produces a higher error σ in the prediction of the concentration profiles but does not drastically change the predicted free-energy profile in *A*. The diffusivity profile in *B* is more susceptible to data reduction. (*C*) Resulting concentration profiles compared with experimental data.